Journal of
Mechanical
Science and
Technology

Journal of Mechanical Science and Technology 21 (2007) 1415~1424

Numerical Simulation of Vortex-induced Vibration of a Square Cylinder

Zhongdi Su*, Yu Liu, Hongjun Zhang, Dongfei Zhang

College of Metrology and Measurement Engineering, China Jiliang University, Hangzhou, 310018, China

(Manuscript Received December 15, 2006; Revised April 25, 2007; Accepted May 2, 2007)

Abstract

Vortex-induced vibration (VIV) of a square cylinder in a cross flow is examined numerically. Both the rigid and elastic cases are simulated at a low Reynolds number of 100. The approach solves the unsteady flow field using a finite element method with a deforming grid to accommodate the moving cylinders. As for the cylinder motions, a two-degree-of-freedom structural dynamics model is invoked. Fluid-structure interactions are resolved through iteration at the same time step. The calculated results for the case of rigid cylinder indicated that the non-dimensional vortex shedding frequency (or the Strouhal frequency) of a square cylinder at rest is 0.13, which is in good agreement with the published results. For the elastic case, with the change of the cylinder's natural frequency, "lock-in" and "beat" phenomena were successfully captured. The phenomena of resonance and galloping can also be indicated.

Keywords: Vortex-induced vibration; Lock-in; Beat; Resonance; Galloping

1. Introduction

Vortex shedding behind bluff bodies arises in many fields of engineering, such as heat exchanger tubes, marine cables, flexible risers in petroleum production and other marine applications, bridges, and chimneys stacks. These examples are only a few of a large number of problems where vortex-induced vibrations are crucial. Vortex-induced vibration of a square cylinder is one of the fundamental problems in flow-induced vibration. For a cylinder in a cross flow, the flow separates and vortex streets are formed in the wake of the cylinder when the Reynolds number exceeds a critical value. The vortices are alternately shed from the cylinder. This vortex shedding induces an approximately periodic excitation on the cylinder and causes it to vibrate. The structural vibration modifies the flow, which in turn alters the induced force acting on the cylinder. The resulting fluid-structure interaction is a non-linear process and will give rise to structural vibration with multiple frequencies (Blevins, 1994; Blake, 1986).

Experiment is an effective way to study the problem of vortex-induced vibration of a bluff cylinder. Zhang *et al.* (2003) experimentally studied the fluid damping of a long slender cylinder, fixed at both ends (no rotation and displacement), in a cross flow. The structural dynamic strain was measured in the transverse direction over a range of reduced velocity U_r using a fibre-optic Bragg grating sensor. The results showed that the value of fluid damping varied significantly at resonance when the vortex-shedding frequency coincided with one of the natural frequencies of the combined fluid–structure system. Govardhan and Williamson (2004) study the transverse vortex-induced vibrations of a cylinder at low mass-damping values. For large mass ratios, m^*=O(100), the vibration frequency for synchronization lies close to the natural frequency ($f^* = f/f_n \sim$

*Corresponding author. Tel.: +86 571 8691 4542, Fax.: +86 571 8683 6061
E-mail address: suzhongdi@cjlu.edu.cn

1.0), but as mass is reduced to m^*=O(1), f^* can reach remarkably large values. Lam *et al.* (2004) experimentally investigated the effects of surface waviness of cylinders on mean drag and fluctuating lift reduction. Marcollo and Hinwood (2006) designed a new experimental facility to investigate the vortex-induced vibration of a long flexible cylinder. The response of a freely oscillating circular cylinder (''free vibration'') in cross-flow has been also studied experimentally by Klamo *et al.* (2005), using controlled magnetic eddy current to provide variable damping. The main objective of the study is to characterize the maximum amplitude that is achieved for a given system as cross-flow velocity varies. The maximum amplitude occurs within a small range of the effective stiffness of the system. Hover *et al.* (2004) experimentally investigated three-dimensionality of mode transition in vortex-induced vibrations of a circular cylinder. Jauvtis and Williamson (2003) studied the response of an elastically mounted cylinder, which is free to move in two degrees of freedom in a fluid flow, and which has low mass and damping. They found that, surprisingly, the freedom to move in two directions has very little effect on the transverse response, the modes of vibration, or the vortex wake dynamics.

Vortex-induced vibration of a bluff cylinder has also been numerically studied. Wang *et al.* (2003) studied the flow-induced vibration of an Euler-Bernoulli beam. Using the method of direct numerical simulations (DNS), Dong and Karniadakis (2005) studied the turbulent flows past a stationary circular cylinder and past a rigid cylinder undergoing forced harmonic oscillations at Reynolds number Re =10000. Guilmineau and Queutey (2004) presented some numerical results from a study of the dynamics and fluid forcing on an elastically mounted rigid cylinder with low mass-damping, constrained to oscillate transversely to a free stream. The incompressible two-dimensional Reynolds-Averaged Navier–Stokes (RANS) equations are used to investigate the vortex shedding around the cylinder numerically. Several initial conditions are also used. According to the initial condition, the simulations predict correctly the maximum amplitude. Leontini *et al.* (1999) conducted a two-dimensional simulations of flow past both an elastically mounted cylinder and an externally driven oscillating cylinder at a Reynolds number of Re = 200. The numerical study has shown that the driven oscillating system is highly sensitive to the amplitude of oscillation, and the oscillation frequency, especially in the region of parameter space where VIV occurs. Wanderley and Levi (2002) simulated the process of vortex-induced vibrations on a circular cylinder, using a finite difference method. The numerical solution provided a close picture of the real physics of the phenomenon including the Karman vortex street and its effect on the oscillation behavior of the lift and drag coefficients due to the asymmetric pressure distribution around the cylinder. Al-Jamal and Dalton (2004) performed a 2-D LES study of the VIV response of a circular cylinder at a Reynolds number of 8000 with a range of damping ratios and natural frequencies. The results show the expected vibratory response of the cylinder for $0.555 < f_{st} / f_n < 1.59$, where f_{st} is the non-vibrating vortex-shedding frequency and f_n is the natural frequency. For a solid cylinder with a mass factor (m^*) of 7.85 and a material-damping ratio of 0.02, lock-in was observed for $0.793 < f_{st} / f_n < 1.39$ with a peak at a reduced velocity of 5.5. Liu *et al.* (2003) numerically simulated the vortex-induced vibrations of two side-by-side circular cylinders in a cross flow at low Reynolds numbers. The cylinders, of low non-dimensional mass (m^*=10), are free to vibrate in both the transverse and in-line directions.

Sarpkaya (2004) summarized a comprehensive review of the progress made during the past two decades on vortex-induced vibration (VIV) of mostly circular cylindrical structures subjected to steady uniform flow. Gabbai and Benaroya (2005) reviewed the literature on the mathematical models used to investigate vortex-induced vibration (VIV) of circular cylinders. Compared to many studies about the circular cylinder, fewer studies have been undertaken for the VIV of a square cylinder. Some differences between the two geometries can be expected. It is well known that flow separations associated with these cylinders are different, i.e. the circular cylinder are associated with oscillating separating points while the square cylinder has fixed flow separation points. As a typical bluff body, the characteristic of the VIV of square cylinder is significant to be studied. In this paper, flow-induced vibration of a square cylinder in a cross flow is examined numerically. Two different cases are considered: one is rigid case where the structural stiffness of the cylinder is assumed to be infinite, and other is the elastic case where the cylinder undergoes oscillations. In the latter case, the cylinder vibrates under the action of the unsteady

flow-induced force. Both cases are simulated at a Reynolds number of 100. The approach solves the unsteady flow field using a finite element method with a deforming grid to accommodate the moving cylinders. As for the cylinder motions, a two-degree-of-freedom structural dynamics model is invoked. Fluid-structure interactions are resolved through iteration at the same time step. For the elastic case, the cylinder is allowed to vibrate in the transverse directions. The non-dimensional mass ratio of the cylinder is m^*= 10. To encourage high-amplitude oscillations, the structural damping coefficient ζ_s is set to zero. Different natural frequencies of the cylinder are selected to calculate.

2. Computational methods

2. 1 Flow calculation

The two-dimensional computation domain is a *60D* ×*20D* rectangular region, the upstream length is about *10D*, while the downstream length is *50D*, and the cylinder is symmetric about the centerline (Fig. 1).

The non-dimensional governing equations are given for ease of reference:

$$\frac{\partial u_i}{\partial x_i}=0\,, \tag{1}$$

$$\frac{\partial u_i}{\partial \tau}+u_j\frac{\partial u_i}{\partial x_j}=\frac{\partial \sigma_{ij}}{\partial x_i}\,,\quad i,j=1,2,3 \tag{2}$$

and

$$\sigma_{ij}=-p\delta_{ij}+\frac{1}{Re}\left(\frac{\partial u_i}{\partial x_j}+\frac{\partial u_j}{\partial x_i}\right), \tag{3}$$

A finite element method was used to solve the Navier-Stokes equation. The non-linear coupling terms in the equations are treated separately at different fractional time steps, by an operator splitting time stepping method. The method is suitable for both steady and transient problems. It can readily be extended to include extra equations describing additional physical effects, such as the effects of the cylinder motions on the flow field and vice versa (Bristeau *et al.*, 1987).

With the superscript m denoting the iteration number, the steps involved in generating the solution (u_i^{m+1}, p^{m+1}) are as follows:

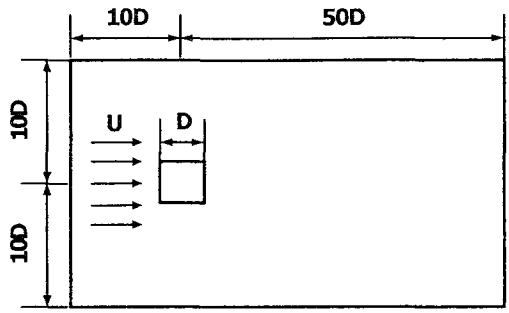

Fig. 1. Flow past a square cylinder.

(a) First fractional step:

$$\frac{u_i^{m+\gamma}-u_i^{m}}{\delta\Delta\tau}-\frac{\alpha}{Re}\frac{\partial^2 u_i^{m+\gamma}}{\partial x_j\partial x_j}+\frac{\partial p^{m+\gamma}}{\partial x_i}=\frac{\beta}{Re}\frac{\partial^2 u_i^{m}}{\partial x_j\partial x_j}-u_j^{m}\frac{\partial u_i^{m}}{\partial x_j}\,, \tag{4}$$

$$\frac{\partial u_i^{m+\gamma}}{\partial x_i}=0\,. \tag{5}$$

(b) Second fractional step:

$$\frac{u_i^{m+1-\gamma}-u_i^{m+\gamma}}{(1-2\delta)\Delta\tau}-\frac{\beta}{Re}\frac{\partial^2 u_i^{m+1-\gamma}}{\partial x_j\partial x_j}+u_j^{m+1-\gamma}\frac{\partial u_i^{m+1-\gamma}}{\partial x_j}=-\frac{\alpha}{Re}\frac{\partial^2 u_i^{m+\gamma}}{\partial x_j\partial x_j}-\frac{\partial p^{m+\gamma}}{\partial x_i}\,. \tag{6}$$

(c) Third fractional step:

$$\frac{u_i^{m+1}-u_i^{m+1-\gamma}}{\delta\Delta\tau}-\frac{\alpha}{Re}\frac{\partial^2 u_i^{m+1}}{\partial x_j\partial x_j}+\frac{\partial p^{m+1}}{\partial x_i}=\frac{\beta}{Re}\frac{\partial^2 u_i^{m+1-\gamma}}{\partial x_j\partial x_j}-u_j^{m+1-\gamma}\frac{\partial u_i^{m+1-\gamma}}{\partial x_j}\,, \tag{7}$$

$$\frac{\partial u_i^{m+1}}{\partial x_i}=0\,. \tag{8}$$

In the above schemes, $\alpha,\beta\in(0,1)$, and $\alpha+\beta=1$, $\gamma\in(0,1/3)$.

The sub-problems at first and third fractional steps are of the type of steady Quasi-Stokes (QS) problem. It can be solved by a pre-conditioned conjugate gradient method. The sub-problem at second

fractional step is of the type of classical nonlinear diffusion-convection problem (NL). The sub-problem (NL) can be reformulated as a least square problem and solved by a pre-conditioned conjugate gradient method.

Since the boundary layer is expected to be thin near the cylinder, a fine mesh is specified near the cylinder surface. 6-noded triangular element is used. The number of nodes is 99506, and the number of elements is numerically determined to be 49506, which is adequate to resolve the velocity and the boundary layers. These numbers are determined by using different meshes, from coarser to progressively finer meshes, until the drag coefficient is convergent to within a prescribed tolerance of 0.5%.

2.2 Cylinder dynamics

It is assumed that the square cylinder is rigidly mounted. The long cylinder is modeled as a spring-damper-mass system, which is representative of the location of maximum amplitude of vibration at the mid-section of a long cylindrical structure mounted with fixed ends. Thus, the motions of cylinder are calculated by solving a two-degree-of-freedom dynamic equation:

$$\frac{d^2X_i}{d\tau^2}+\frac{4\pi\zeta_s}{U_r}\frac{dX_i}{d\tau}+(\frac{2\pi}{U_r})^2X_i=\frac{F_i}{2m^*}, \tag{9}$$

where X_i = (X, Y) denote the instantaneous non-dimensional displacements of the cylinders in the x- and y- directions respectively, ζ_s is the non-dimensional structural damping coefficient, $m^*= m / (\rho D^2)$ is the mass ratio, m is the mass per unit length, F_i = (C_D, C_L) is the non-dimensional force, i.e. force coefficient, D is the characteristic length of the cylinder and U_r is the reduced velocity. The reduced velocity is an important parameter relating the structural vibration frequency to the D and the U, the income velocity. It is defined as

$$U_r=\frac{U}{f_nD}, \tag{10}$$

where f_n is the natural frequency of the stationary cylinder. The solution yields the vibration displacement and the velocity of the cylinder as they respond to the surrounding flow field. The incompressible flow solution procedure is coupled with the cylinder response, thus allowing the fluid-structure interactions to be adequately resolved at each time step.

2.3 Fluid-structure coupling

Solving fluid-structure interaction problems generally involves moving computational domains and dynamic re-meshing. With this arrangement, the elastic cylinder is free to vibrate within the flow domain. Therefore, a deforming computational mesh is required to accommodate the arbitrary motion of the elastic cylinders. The surfaces of the cylinders are adjusted according to the motion of the cylinders by means of nodal displacement. At each time step the displacements of cylinder are calculated, represented by X_i = (X, Y). In order to distribute the mesh deformation as uniformly as possible, i.e. to minimize local mesh deformation, a Laplacian equation of displacement is solved throughout the computational domain with the displacements of cylinder the boundary condition. The entire computational mesh is adjusted by a Laplacian interpolation, which is designed to map a mesh smoothly onto a reasonably similar shape, specified by the displacements of the elastic cylinder.

During the calculation, the reference frame is fixed on the far field. The cylinder is free to vibrate within the calculation domain. At each time step, the fluid flow is solved using the finite-element method (FEM).

The instantaneous drag F_D and lift F_L acting on the cylinder is calculated by integrating the pressure and the wall shear stress on the surface. Their corresponding coefficient is defined as $C_D=2F_D /\rho U_\infty^2 D$ and $C_L=2F_L/\rho U_\infty^2 D$, respectively. This is then taken as the force input for Eq. (9) and the response of the cylinder is calculated by solving Eq. (9) using the Runge-Kutta method. The cylinder is moved according to the displacement, and the mesh is remapped according to this motion. Then the flow field is solved again using the cylinder velocity as the boundary condition. Finally, the whole process is repeated in an iterative way so that the interactions between the fluid and the cylinder are accounted for properly.

3. Results and discussions

3.1 Flow pasts a stationary cylinder

Computations for a stationary cylinder at Re =100

are carried out till the flow reaches a stationary solution. The calculated Strouhal number *St*, mean drag coefficient $\overline{C_D}$ and the root mean square value of the lift coefficient $C_{L,rms}$ are 0.132, 1.296 and 0.1196, respectively. The present results are compared with some of the published experimental and calculated results in Table 1. Our results of $\overline{C_D}$, $C_{L,rms}$ and *St* consist with the reported data well. The differences between the present calculation and the published results are very small. As shown in Fig. 2(a), the time series of C_L turns to be periodic after t = 200, where t is the non-dimensional time, indicating a stationary state. The power spectrum of C_L is shown in Fig. 2(b). Here, E_L is the power spectral density, which is defined as the square norm of system function scaled by the sampling interval and white-noise variance. The power spectrum of C_L has only one peak, indicating a single vortex shedding frequency. The Strouhal number is the non-dimensional vortex shedding frequency, that we can also call it Strouhal frequency.

Table 1. Comparisons of the engineering parameters for flow past a square cylinder at Re = 100.

	$\overline{C_D}$	$C_{L,rms}$	*St*
The present results	1.296	0.120	0.132
Okajima (1982, exp)	-	-	0.135
Breuer *et al.* (2000, cal)	1.38	-	0.138
Bernsdorf *et al.* (1998, cal)	1.38	-	0.138
Guo *et al.* (2003, cal)	1.33	-	0.133
Wang *et al.* (2003, cal)	1.403	0.127	0.1353

3.2 Flow pasts an elastic cylinder

For the elastic case, the cylinder is allowed to vibrate in the transverse directions. The non-dimensional mass ratio of the cylinder is m^*= 10. To encourage high-amplitude oscillations, the structural damping coefficient ξ is set to zero. Different natural frequencies of the cylinder are selected to calculate.

3.2.1 The captured special phenomena of vortex-induced vibration (VIV)

The vortex shedding frequency of a stationary cylinder has been calculated, f_{st} = 0.132. Changing the natural frequency of the square cylinder, some typical modes of VIV are captured. The time series of C_L and *Y/D* (*Y* is the transverse displacement, *D* is the length of side) with different frequency ratios, f_{st}/f_n = 0.5, 0.875, 1.125 and 1.25 are shown in Fig. 3. When f_{st}/f_n = 0.5, the time series of C_L and *Y/D* fluctuate periodically. The amplitude of *Y/D* is very small, less than 0.01, indicating a weak vibration induced by vortex shedding. Increasing the frequency ratio to 0.875, a stronger vibration is obtained. The time series of *Y/D* exhibits a special character. The amplitude periodically changes with time, indicating that the cylinder is vibrating with multiple frequencies. This is the so-called "beat" mode of VIV. For this frequency ratio, the highest amplitude of *Y/D* can reach 0.07, while the lowest is only about 0.01. As the frequency ratio is increased further to 1.125, another typical VIV mode appears, that is "lock-in" mode. In this mode, the vibration frequency is locked in the natural frequency of the structure. The time series of *Y/D* fluctuates periodically with a stationary high-amplitude of 0.06. When f_{st}/f_n is increased to 1.25, "beat" mode appears again. "Beat" and "lock-

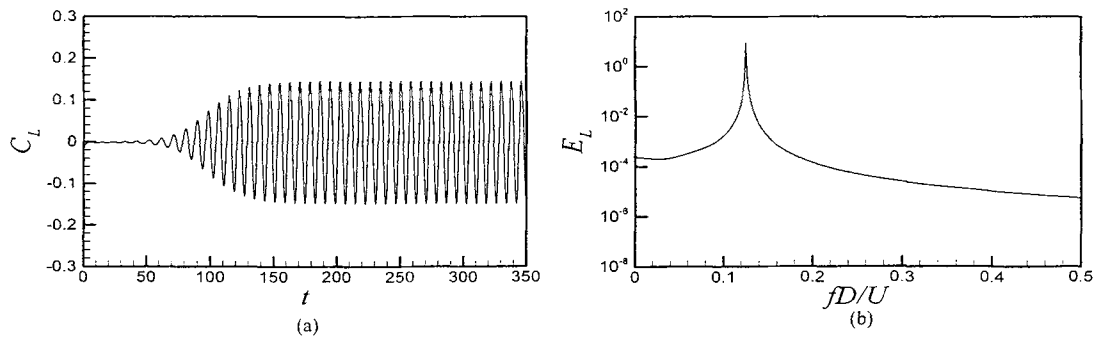

Fig. 2. The stationary cylinder at Re =100; (a) C_L time series; (b) power spectra of C_L.

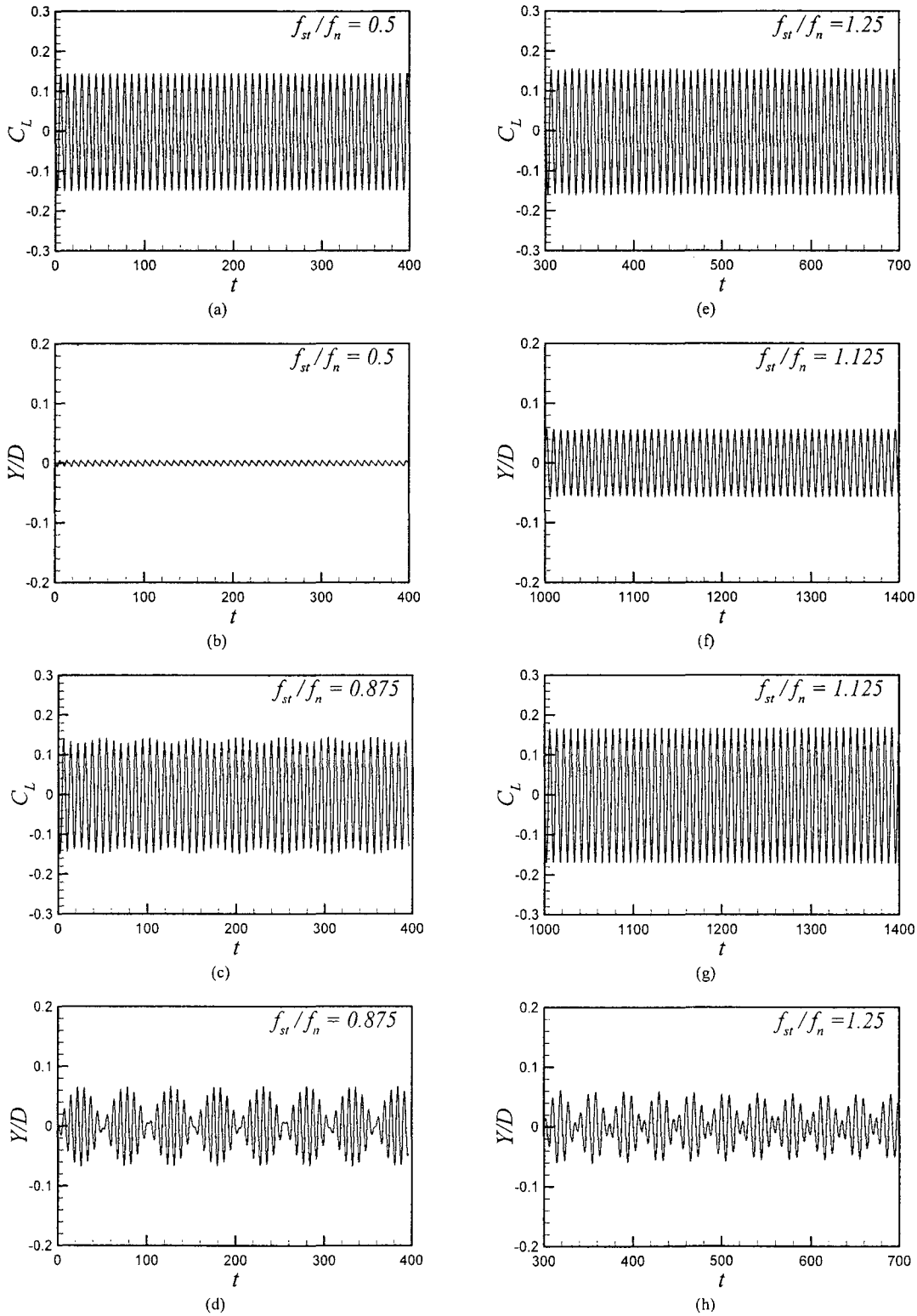

Fig. 3. Time series of C_L and Y/D with different f_{st}/f_n.

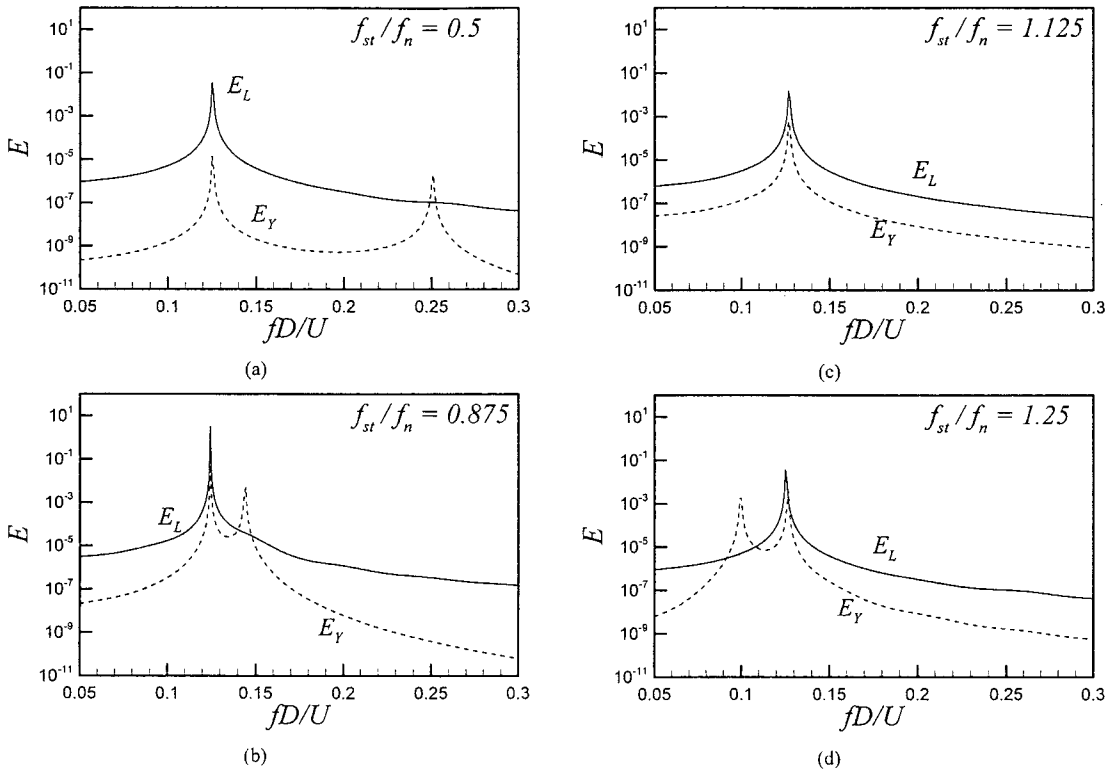

Fig. 4. Power Figure 4 Power spectra of C_L and Y/D with different f_{st}/f_n.

in" are two typical modes of VIV, which have been recorded, as indicated in Sarpkaya (2004), Gabbai and Benaroya (2005).

To clarify the relation between the vortex shedding frequency and the vibration frequency, the power spectra of C_L and Y/D with the frequencies ratios of 0.5, 0.875, 1.125 and 1.25 are shown in Fig. 4. When f_{st}/f_n = 0.5, 0.875 and 1.25, the power spectra of C_L have one peak only, which corresponds to the vortex shedding frequency. But the power spectra of Y/D have two peaks, indicating two main vibration frequencies, one is the vortex shedding frequency, another is the natural frequency. When "lock-in" mode appears at f_{st}/f_n = 1.125, the power spectra of C_L and Y/D both have single peak at the same frequency. At this time, the vibration frequency and vortex shedding frequency are locked in the natural frequency.

3.2.2 Discussion for resonance and galloping

In the calculation, two maximal amplitude vibration modes are captured at some special frequency ratios. Compared to the normal VIV modes presented above, the amplitude of the vibration can reach a much higher level. In these maximal amplitude vibration cases, the calculation can no longer be iteratively carried out because of the significant mesh deformation, so we didn't get the ultimate stationary vibration state. But, according to the maximal vibration trend, it can be conjectured that resonance or galloping happened.

According to the knowledge of physics, when the natural frequency is very close to the excitation frequency, resonance may occur. This is attested by the calculated results. As the frequency ratio closing to 1.0, an obvious high-amplitude vibration appears, and the calculation is interrupted. Figure 5 shows the time series of Y/D, while f_{st}/f_n is 0.975 and 1.0, respectively. The largest displacement ratio Y/D can reach 0.3~0.4, that is much higher than the value of normal cases mentioned above.

When the frequency ratio is larger than a critical value, another maximal vibration mode is captured. That must be caused by galloping. Galloping is another causation to induce highest-amplitude vibration.

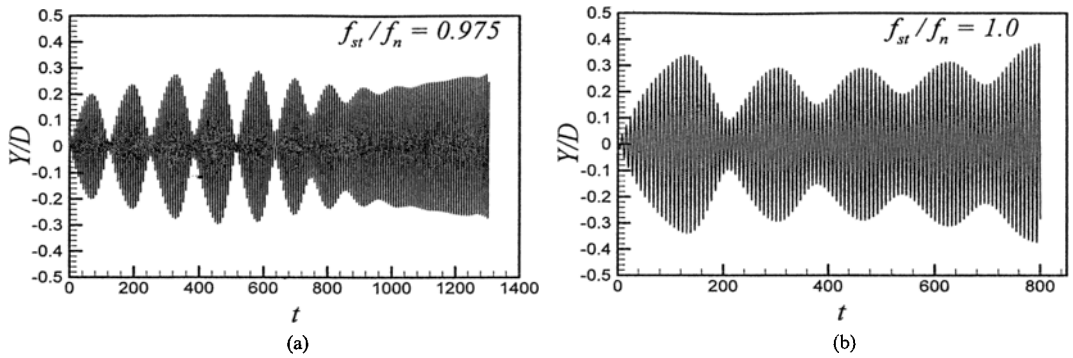

Fig. 5. Time series of Y/D, while $f_{st}/f_n = 0.975$ and 1..

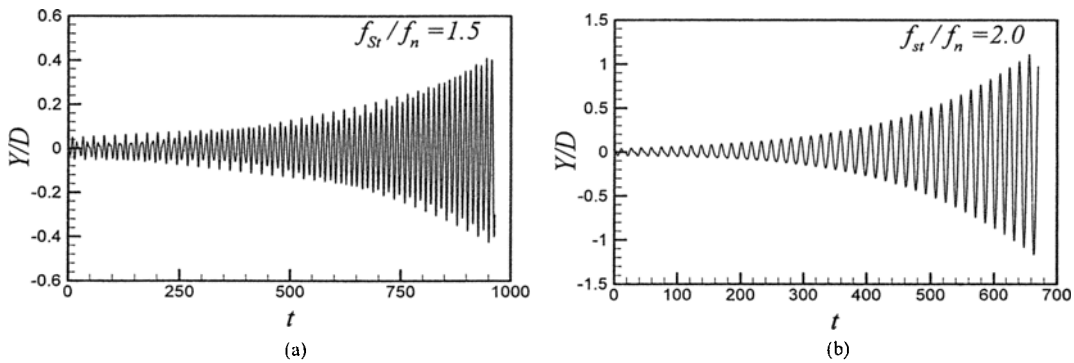

Fig. 6. Time series of Y/D, while $f_{st}/f_n = 1.5$ and 2.0.

It is understood that galloping vibration is not a phenomenon of VIV. It arises from fluid forces induced by structural vibration in a fluid flow. That is a strong vibration at a lower frequency, compared to vortex shedding frequency. In the calculations, while the frequency ratio f_{st}/f_n is larger than 1.5, galloping mode is got. Figure 5 shows the time series of Y/D, while f_{st}/f_n is 1.5 and 2.0. Unlike the resonance process, the amplitude of vibration is always increasing from the beginning. Because of the interruption in calculation, the ultimate stationary state of galloping are not captured, but the vibration trends are in good agreement with Sarpkaya (2004).

3.2.3 The vibration modes of a square cylinder

In this study, 12 cases with different natural frequency are calculated. Variation of the maximum transverse displacement of the cylinder with different frequency ratios is shown in Fig. 7. Varying f_{st}/f_n from 0.5 to 2.0, the vibration of the cylinder changing in 6 phases and 5 vibration modes are captured, which have been marked in Fig. 7.

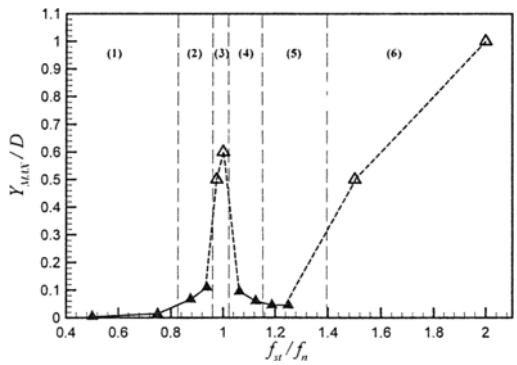

Fig. 7. Variation of the maximum transverse displacement of the cylinder with different frequency ratios.

(1) Low-amplitude vibration. While the frequency ratio is in region 1, the vibration induced by flow is very weak, the amplitude is small and fixed.

(2) "Beat" mode vibration. In region 2, "beat" mode is caused by vortex shedding. The vibration amplitude periodically changes with time.

(3) Resonance. In region 3, resonance is captured.

The cylinder vibrates with a very high amplitude, inducing interruption of the calculation. The amplitudes in this frequency range are conjectured according to the values before the interruption. So the symbols in the figure are unfilled.

(4) "Lock-in" mode vibration. In region 4, the vibration frequency and vortex shedding frequency are locked in the natural frequency. The amplitude turns to be fixed.

(5) "Beat" mode vibration. Further increasing the frequency ratios, "beat" mode appears again in region 5.(6) Galloping. When the frequency ratio increased bigger than 1.5, the highest amplitude is resulted from Galloping.

4. Conclusions

Vortex-induced vibrations of a square cylinder, at low Reynolds number of 100, are examined numerically via a stabilized finite element method applied to the incompressible flow equations in primitive variables. Both the rigid and elastic cases had been studied.

The calculated results for the case of rigid cylinder indicated that the Strouhal frequency of a square cylinder at rest is 0.13, which is in good agreement with the published results.

For the elastic case, with the change of the natural frequency of cylinder, many typical vibration caused by flow are captured. The "lock-in" and "beat" modes are successfully simulated. The resonance and galloping are also indicated. Varying f_{st}/f_n from 0.5 to 2.0, the vibration of the cylinder changes in 6 phases and 5 vibration modes are captured.

Acknowledgement

Supports given by the Zhejiang Natural Science Foundation under grant No. Y604559 are gratefully acknowledged.

References

Al-Jamal, H. and Dalton, C., 2004, "Vortex Induced Vibrations using Large Eddy Simulation at a Moderate Reynolds Number," *Journal of Fluids and Structures*, Vol. 19, pp. 73~92.

Bernsdorf, J., Zeiser, T., Brenner, G. and Durst, F., 1998, "Simulation of 2D Channel flow Around a Square Obstacle with Lattice-Boltzmann (BGK) Automata," *International Journal of Modern Physics C*, Vol. 9 (8), pp. 1129~1141.

Blevins, R. D. 1994, "Flow-Induced Vibration," 2nd Edition, Krieger, New York.

Blake, W. K., 1986, "Mechanics of Flow-Induced Sound and Vibration," *Academic*, New York.

Breuer, M., Bernsdorf, J., Zeiser, T. and Durst, F., 2000, "Accurate Computations of the Laminar flow past a Square Cylinder based on two Different Methods: Lattice-Boltzmann and Finite Volume," *International Journal of heat and fluid flow*, Vol. 21, pp. 186~196.

Bristeau, M. O., Glowinski, R. and Periaux, J., 1987, "Numerical Methods for the Navier-Stokes Equations: Applications to the Simulation of Compressible and Incompressible Viscous Flows," *Computer Physics Reports*, Vol. 6, pp. 73~187.

Dong, S. and Karniadakis, G. E., 2005, "DNS of flow past a Stationary and Oscillating Cylinder at Re = 10000," *Journal of Fluids and Structures*, Vol. 20, pp. 519~531.

Gabbai, R. D. and Benaroya, H., 2005, "An Overview of Modeling and Experiments of Vortex-Induced Vibration of Circular Cylinders," *Journal of Sound and Vibration*, Vol. 282, pp. 575~616.

Govardhan, R. and Williamson, C. H. K. 2004, "Critical mass in Vortex-Induced Vibration of a Cylinder," *European Journal of Mechanics B/Fluids*, Vol. 23, pp. 17~27.

Guilmineau, E. and Queutey, P., 2004, "Numerical Simulation of Vortex-Induced Vibration of a Circular Cylinder with Low Mass-Damping in a Turbulent flow," *Journal of Fluids and Structures*, Vol. 19, pp. 449~466.

Guo, W. B., Shi, B. C. and Wang, N. C., 2003, "Lattice-BGK Simulation of a Two-Dimensional Channel flow Around a Square Cylinder," *Chinese Physics*, Vol. 12 (1), pp. 67~74.

Hover, F. S., Davis, J. T. and Triantafyllou, M. S., 2004, "Three-Dimensionality of mode Transition in Vortex-Induced Vibrations of a Circular Cylinder," *European Journal of Mechanics B/Fluids*, Vol. 23, pp. 29~40.

Jauvtis, N. and Williamson, C. H. K., 2003, "Vortex-Induced Vibration of a Cylinder with two Degrees of Freedom," *Journal of Fluids and Structures*, Vol. 17, pp. 1035~1042

Klamo, J. T., Leonard, A. and Roshko, A., 2005, "On the Maximum Amplitude for a Freely Vibrating Cylinder in Cross-flow," *Journal of Fluids and Structures*, Vol. 21, pp. 429~434.

Lam, K., Wang, F. H. J., Li, Y. and So, R. M. C., 2004, "Experimental Investigation of the Mean and Fluctuating Forces of Wavy(varicose) Cylinders in a Cross-flow," *Journal of Fluids and Structures*, Vol. 19, pp. 321~334.

Leontini, J. S., Stewart, B. E., Thompson, M. C. and Hourigan, K., 2006, "Predicting Vortex-Induced Vibration from Driven Oscillation Results," *Applied Mathematical Modelling*, Vol. 30, pp. 1096~1102.

Liu, Y., So, R. M. C., Lau Y. L. and Zhou, Y., 2003, "Numerical Studies of two Side-by-side Elastic Cylinders in a Cross-flow," *Journal of Fluids and Structures*, Vol. 15, pp. 1009~1030.

Marcollo, H. and Hinwood, J. B., 2006, "On Shear Flow Single Mode Lock-in with both Cross-flow and In-line Lock-in Mechanisms," *Journal of Fluids and Structures*, Vol. 22, pp. 197~211.

Okajima, A., 1982, "Strouhal Numbers of Rectangular Cylinders," *Journal of Fluid Mechanics* Vol. 123, pp. 379~398.

Sarpkaya, T., 2004, "A Critical Review of the Intrinsic Nature of Vortex-Induced Vibrations," *Journal of Fluids and Structures*, Vol. 19, pp. 389~447.

Wang, X. Q., So, R. M. C. and Liu, Y., 2003, "Flow-Induced Vibration of an Euler-Bernoulli Beam," *Journal of Sound and Vibration*, Vol. 243, pp. 241~268.

Wanderley, J. B. V. and Levi, C. A., 2002, "Validation of a Finite Difference Method for the Simulation of Vortex-Induced Vibrations on a Circular Cylinder," *Ocean Engineering*, Vol. 29, pp. 445~460.

Wang, G. C., Shi, B. C. and Deng, B., 2003, "Simulation of flow past Square Cylinders with a Non-Uniform Lattice Boltzmann Method," *Journal of Basic Science and Engineering*, Vol. 11 (4), pp. 335~344.

Zhang, H. J., Zhou, Y., So, R. M. C., Mignolet, C. M. P. and Wang, Z. J., 2003, "A note on the Fluid Damping of an Elastic Cylinder in a Cross-flow," *Journal of Fluids and Structures*, Vol. 17, pp. 479~483.